Planetary boundary layer height retrieval from a diode-laser-based high spectral resolution lidar

Luke Colberg,* Owen Cruikshank, and Kevin S. Repasky
Montana State University, Electrical and Computer Engineering Department, Bozeman, Montana, United States

Abstract. The planetary boundary layer height (PBLH) is an essential parameter for weather forecasting and climate modeling. The primary methods for obtaining the PBLH include radiosonde measurements of atmospheric parameters and lidar measurements, which track aerosol layers in the lower atmosphere. Radiosondes provide the parameters to determine the PBLH but cannot monitor changes over a diurnal cycle. Lidar instruments can track the temporal variability of the PBLH and account for spatial variability when operated in a network configuration. The networkable micropulse DIAL (MPD) instruments for thermodynamic profiling are based on diode-laser technology that is eye-safe and cost-effective and has demonstrated long-term autonomous operation. We present a retrieval algorithm for determining the PBLH from the quantitative aerosol profiling capability of the high spectral resolution channel of the MPD. The PBLH is determined using a Haar wavelet transform (HWT) method that tracks aerosol layers in the lower atmosphere. The PBLH from the lidar is compared with the PBLH determined from potential temperature profiles from radiosondes. In many cases, good agreement among the PBLH retrievals was seen. However, the radiosonde retrieval often missed the lowest inversion layer when several layers were present, while the HWT could track the lowest layer. © *The Authors. Published by SPIE under a Creative Commons Attribution 4.0 International License. Distribution or reproduction of this work in whole or in part requires full attribution of the original publication, including its DOI.* [DOI: 10.1117/1.JRS.16.024507]

1 Introduction

The planetary boundary layer (PBL) is the lowest layer in the Earth's atmosphere that is affected by the surface conditions on the time scale of an hour,[1] with the PBL height (PBLH) defined as the altitude of the top of the PBL. The PBLH follows a diurnal cycle driven by the sensible heat flux of the earth's surface[2] and helps control the exchange of heat, water vapor, aerosols, and momentum between the surface and the free troposphere. The PBLH is an important parameter for meteorological phenomena, including turbulent mixing, convective transfer, and cloud entrainment. It is also an important parameter in creating numerical weather forecasting models,[3–5] estimating surface emissions of trace gases,[6] and predicting the density of surface pollutants.[7,8] Continuous monitoring of the PBLH is advantageous for improving weather forecasting and predicting air quality.

Despite its importance in weather forecasting and climate science, current instrumentation fails to monitor the PBLH adequately. Twice-daily radiosondes from the global radiosonde network fail to capture the temporal variability and diurnal cycle of the PBLH. More recently, remote sensing of the atmosphere with lidar instruments has provided the opportunity to capture the temporal variability of the PBLH.[9–12] The PBLH can be located in a lidar profile because the inversion layer that defines the PBLH is colocated with a steep gradient in a passive tracer such as aerosol concentration or water vapor number density. Several methods exist for determining the PBLH from aerosol or water vapor profiles, including the gradient method,[13,14] the Haar

---

*Address all correspondence to Luke Colberg, luke.colberg@student.montana.edu

wavelet covariance transformation (HWT) method,[15,16] the curve-fitting method,[17,18] and the variance method.[19,20]

In collaboration with the National Center for Atmospheric Research, researchers at Montana State University are developing micropulse DIAL (MPD) instruments for profiling the lower troposphere, including the PBL and the transition to the free troposphere. The MPD instruments are based on semiconductor technology and provide eye-safe operation. Currently, a network of five MPD instruments for water vapor profiling, two instruments for temperature profiling, and three instruments for high spectral resolution lidar (HSRL) measurements of atmospheric aerosols have been developed. These instruments are cost-effective and have demonstrated long-term unattended operation in networkable configurations that can provide continuous temporal resolution and coarse spatial resolution based on the deployment. As these instruments become available to the larger research community, efforts to improve the instrument performance and data products continue.[21–23]

The PBLH retrieval developed for the MPD instruments utilizes an HWT method. The HWT method searches for regions of abrupt change in the lidar signal. The HWT method is similar to the gradient method because it assumes that the inversion layer at the PBLH will be associated with a steep negative gradient in the aerosol concentration. However, the HWT has the advantage of minimizing the effects of high-frequency noise and can better detect the low-frequency transition between the PBL and the free troposphere.

This paper is organized as follows. Section 2 briefly describes the MPD instrument and the experimental site. Section 3 describes the PBLH retrieval method. Section 4 presents the results, including case studies and radiosonde comparisons. Section 5 discusses the results, and Sec. 6 provides a brief conclusion.

2 Instrumentation

The lidar used for data collection uses the MPD architecture for differential absorption measurements of oxygen in the atmosphere. The off-line wavelength, operating at 770.1085 nm, and a potassium absorption cell are used to provide HSRL measurements of aerosol optical properties. Details regarding this MPD instrument are available in Spuler et al.[24] and Stillwell et al.[25] The aerosol backscatter coefficient is the primary data product used in the PBLH retrieval. Data used in the HSRL retrieval[26] is integrated into 5-min time bins. The pulse duration of the MPD transmitter is 1 μs and corresponds to a 150-m range resolution. The detectors over-sample the laser pulse by a factor of 4, yielding data from a range bin of 37.5 m with an uncertainty of 150 m.

A colocated radiosonde station was used to launch Vaisala RS92-SGP radiosondes for comparison. These radiosondes provide range-resolved atmospheric parameters, including temperature, pressure, and humidity. A total of 32 radiosondes were launched during this study.

The MPD instrument and radiosonde station are located on the campus of Montana State University in Bozeman, Montana (45.6666°N, 111.0460°W). Bozeman is 1524 m above sea level and experiences a dry continental climate typical of the Rocky Mountain region of the western United States. Typically, Bozeman experiences relatively low aerosol optical depths punctuated by episodes of high aerosol loading due to forest fire activity in the western United States and Canada.

3 PBLH Retrieval

The retrieval algorithm presented in this paper uses a series of processing steps to determine the PBLH. The first two steps of the retrieval algorithm include developing a cloud mask to identify clouds and a simple metric to determine the height of the free troposphere, which is used as an upper limit on the range for the remainder of the retrieval. Next, an HWT is applied to the normalized aerosol backscatter coefficient profile and is used to identify the aerosol layers below the height of the free troposphere. This HWT is used in the remaining four steps to identify the capping inversion (CI) layer, identify the bottom of residual layers (RLs), set the top limit for the PBLH retrieval, and finally locate the PBLH. The PBLH retrieval algorithm is compared with potential temperature profiles from colocated radiosondes. Figure 1 shows the PBLH, CI, and
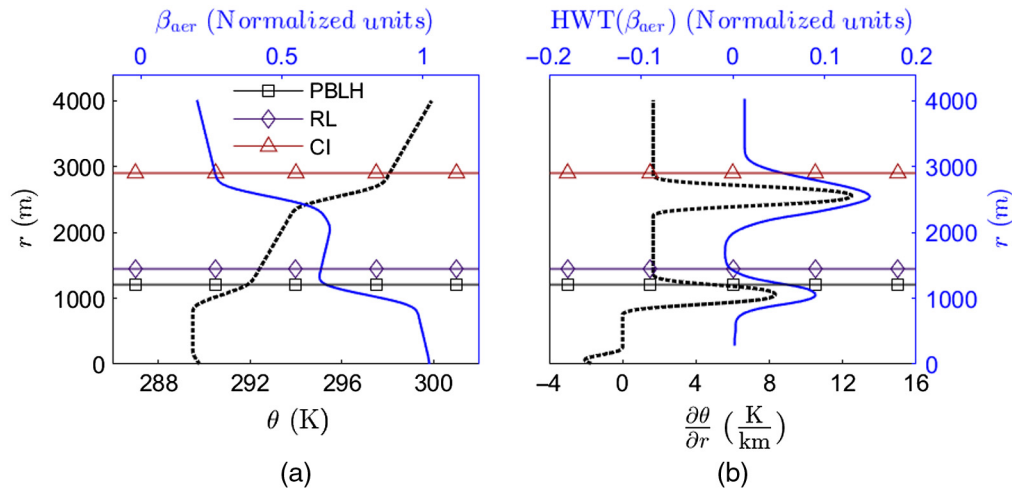
Fig. 1 The PBLH, RL, and CI for typical atmospheric conditions. (a) The aerosol backscatter coefficient (potential temperature) profile as a blue solid (black dotted) line. (b) The HWT of the aerosol backscatter coefficient (potential temperature lapse rate) as the blue solid (black dotted) line.

RL for typical atmospheric conditions. The PBLH and CI are located above regions of steep change in the aerosol backscatter coefficient, β_{aer}, and potential temperature, θ, profiles, which corresponds to maxima in the HWT and potential temperature lapse rate, $\frac{\partial\theta}{\partial r}$, profiles. The RL is associated with an increase in the aerosol backscatter coefficient with range, r, and is located by finding negative HWT values.

The first step in the retrieval algorithm is to identify clouds in the lidar return signal. A cloud masking algorithm based on the method developed by Binietoglou et al.[27] is used to locate clouds in the lidar signal. Specifically, two of the features extraction methods, the Sobel operator and the standard deviation of a 5×5 grid of lidar bins, were used to identify clouds. The Sobel operator detects the edges of clouds, as the edges of clouds are expected to have a much higher gradient than other regions of the lidar signal. The standard deviation method is used to locate the center of clouds, as the variance of the signal within a cloud is much higher than in other regions.

Once the clouds are identified, the next step in the retrieval is to estimate the height of the free troposphere. Low aerosol concentrations characterize the free troposphere, and this height is defined as the height where the aerosol backscatter coefficient initially falls below $5 \cdot 10^{-8}$ m^{-1} sr^{-1}. The purpose of determining the height of the free atmosphere is to set an upper limit to the retrieval for all following layers. Once the height of the free troposphere is found, clouds above this height are not considered, which minimizes the effect of high-altitude clouds.

The next step in the PBLH retrieval is the application of an HWT to the retrieved aerosol backscatter coefficient profile. The aerosol backscatter coefficient profile is first normalized to its average value below 400 m so that the same HWT thresholds can be used in all conditions. The HWT, also known as the wavelet covariance transform (WCT), is used as the basis for the PBLH retrieval and is implemented according to Brooks.[15] The HWT works by convolving a filter function with the normalized aerosol backscatter coefficient profile, which provides a proxy measurement for the aerosol concentration and a passive tracer for the PBLH. The convolution of the filter function and the aerosol backscatter coefficient profile is used to identify large gradients, identifying aerosol transition layers. The filter function, $h(r)$, used for the HWT is

$$h\left(\frac{z-r}{a}\right) = \begin{cases} +1: & r-\frac{a}{2} \leq z \leq r \\ -1: & r \leq z \leq r+\frac{a}{2}, \\ 0: & \text{elsewhere} \end{cases} \tag{1}$$

where r is the range of interest, a is the dilation, and z is a variable that comes into play in the convolution.

Accuracy in the HWT method relies on the correct choice of dilation. Brooks demonstrated that the ideal choice of dilation is equal to the depth of the transition zone at the top of the PBL.[15] Unfortunately, this value is usually not known. However, the depth of the transition zone tends to increase as the PBLH increases in altitude. For this reason, a range-dependent dilation similar to the one used by Baars et al.[10] is used for the retrieval. The dilation used for this work is equal to the altitude of the range bin divided by three and rounded to the nearest multiple of the range bin depth. The dilation reaches a maximum of 900 m at an altitude of 2700 m. Above this altitude, it is constant. A dilation of 150 m is used for any range bin with an altitude <450 m.

The HWT, $H(a, r)$, is found by convolving the filter function with the variable dilation with β_{aer}, so that

$$H(a, r) = \frac{1}{a} \cdot \int_{r-\frac{a}{2}}^{r+\frac{a}{2}} \beta_{\text{aer}}(z) \cdot h\left(\frac{z - r}{a}\right) dz. \tag{2}$$

The HWT, $H(a, r)$, is used to identify aerosol layers and used in the remaining steps of the PBLH retrieval.

The next step in the PBLH retrieval identifies the CI. The CI is the highest altitude with a significant HWT value in the lidar signal below the free troposphere. The CI is set to the highest range bin where the HWT is >0.05, with an upper range limit set at 300 m above the height of the free troposphere layer. If there is a cloud beneath the free troposphere, the CI is the altitude of the maximum HWT value above the cloud.

Identifying the RLs is the next step in the PBLH algorithm. RLs are located and used as a top limiter for the PBLH retrieval in a method similar to that used by Dang et al.[12] Frequently, the inversion layer between the lofted RL and the CI has an HWT value greater than the inversion layer at the PBLH. RLs must be located so that the PBLH retrieval does not errantly set the PBLH to the top of an RL. Different thresholds are used for the RLs depending on the time of day. In the morning, RLs are particularly troublesome because the growing convective layer is frequently beneath the minimum range of the lidar. In the first half of the day, any point in the HWT <0 is identified as an RL. In the evening, RLs are also an issue, as a new PBL forms beneath the well-mixed layer of the previous day. In the last sixth of the day, any point in the HWT < −0.02 is identified as an RL. RLs are not considered for the rest of the day because, during periods of high convection, negative HWT values sometimes occur within the PBL, and searching for RLs causes errors in the PBLH retrieval. The CI is used as the upper limit for where the retrieval algorithm searches for the RL.

The sixth step in the PBLH retrieval algorithm sets an upper range limit for the PBLH retrieval. The presence of RLs increases the variability of PBLH height between lidar and radio-sonde methods when an upper range limit is not used.[28] Figure 2 displays how this limit is
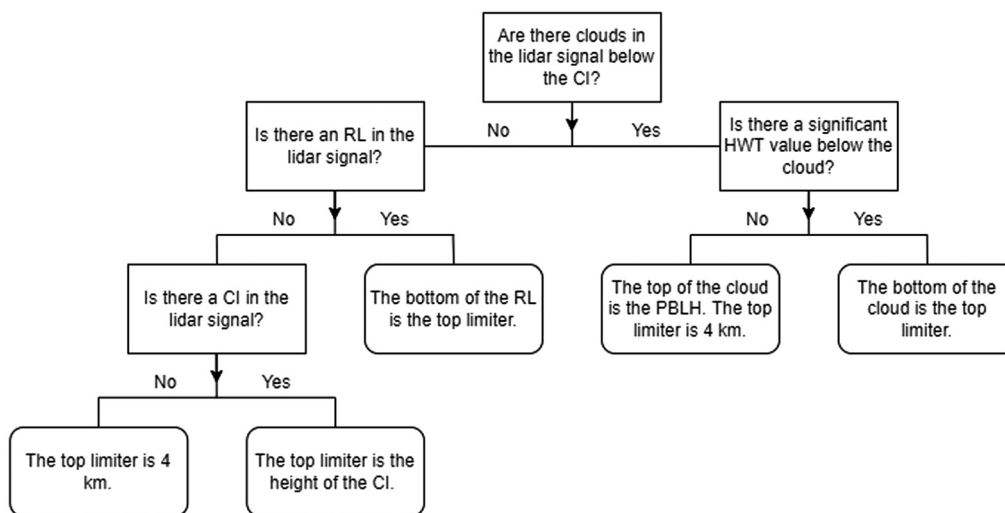

Fig. 2 A flowchart for determining the top limiter in the PBLH retrieval algorithm.

selected. The location of the top limiter is determined by the altitude of the CI, the RLs, and PBL clouds. If there is a cloud beneath the CI, the algorithm searches for an HWT value >0.05 under the cloud base. If one exists, the upper limit is set to be the bottom of the cloud. If the top limiter, as determined by the CI, RLs, and clouds, is higher than 4 km, the upper limit is lowered to 4 km. The lower limit of the lidar signal is considered to be the minimum range of the lidar plus the dilation for the lowest range bins.

The seventh and final step of the PBLH retrieval algorithm identifies the PBLH. If there are no clouds in the lidar signal, the algorithm first searches for a local maximum in the HWT. Then, it places the PBLH at the first point above the peak where the HWT falls below a threshold. The algorithm chooses the lowest peak >0.08 in the HWT. If no point fits this criterion, the algorithm searches for the first peak >0.05 in the HWT. Once this peak is found, the algorithm then sets this peak as the lower limit for searching for the PBLH. The PBLH is then the first point in the HWT that falls below 0.05. If this point does not exist, then the PBLH is set to the altitude of the minimum HWT between the peak and the top limiter. If there is a cloud below the upper limit, the PBLH is set to the altitude of the maximum HWT between the base of the cloud and the top limiter.

The PBLH retrieval steps are shown sequentially in Fig. 3. Figure 3(a) shows the aerosol backscatter coefficient on a logarithmic scale for a single day from sunrise to sunset. Figure 3(b) shows the free atmosphere as green dots. In Fig. 3(c), the CI is displayed as red crosses. The RLs are located beneath the CI and are shown as purple diamonds in Fig. 3(d). In Fig. 3(e), the CI and RLs generate the top limiter, represented as a gray line. In Fig. 3(f), the PBLH is located beneath the top limiter and is shown as black asterisks.

The PBLH retrieval contains many outlying points due to noise in the lidar signal. For this reason, an iterative method was developed for removing outlying points. The first step to the iterative method is taking the 1-h moving average of each layer. Any points >300 m away from
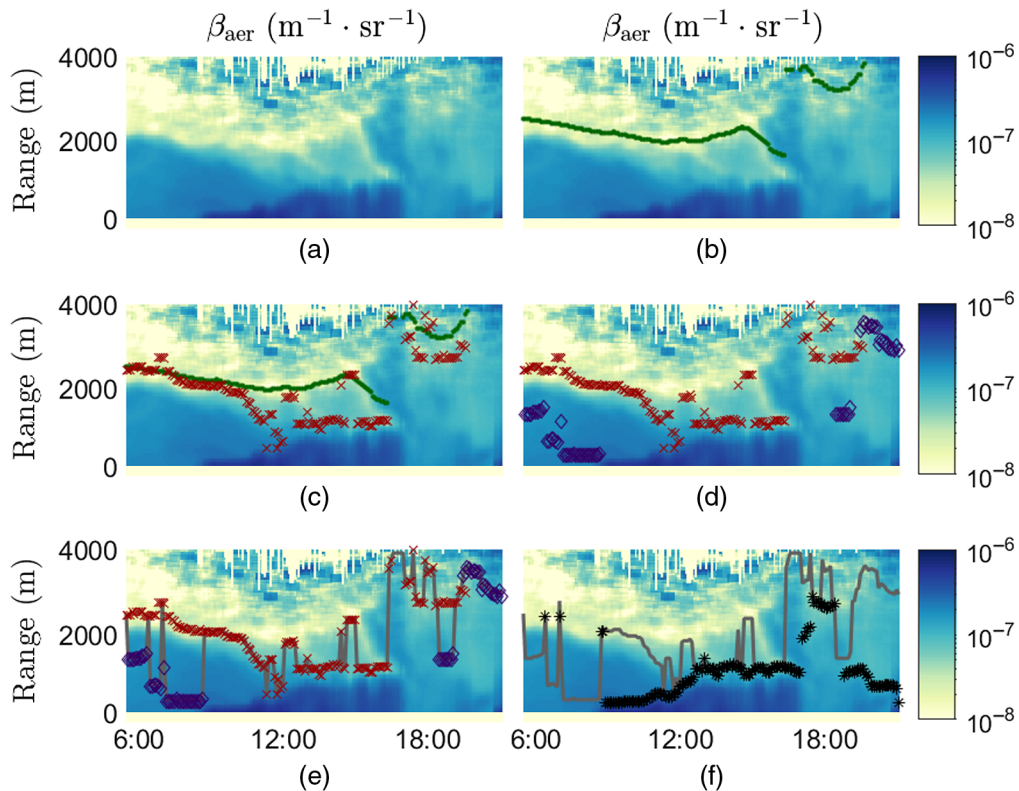

Fig. 3 The atmospheric layers found by the retrieval algorithm. (a) The aerosol backscatter coefficient on a logarithmic scale from sunrise to sunset. (b) The free atmosphere as green dots. (c) The CI as red crosses. (d) The bottom of RLs as purple diamonds. (e) The CI and RLs generate the top limiter, which is represented as a gray line. (f) The PBLH as black asterisks beneath the top limiter.

the moving average are considered potential outliers. The algorithm searches for the closest point that meets each layer's criteria to the moving average. New points are found, and the moving average is recomputed with these new points. If there is no change between iterations, the operation is complete, and the iterative method is terminated.

Validation of the PBLH retrieval using the algorithm described above is achieved by comparing the PBLH retrieved from the potential temperature profiles measured using colocated radiosondes. The Heffter method was used as an objective method for determining the PBLH from the radiosonde profiles, and it was implemented according to the process described by Sivaraman et al.[29] The Heffter method uses the potential temperature lapse rate to locate the PBLH. The Heffter method first defines inversion layers as layers with a potential temperature lapse rate $>5 \frac{K}{km}$ below an altitude of 4 km. Once these inversion layers are located, the Heffter method then looks for the lowest inversion layer with a potential temperature difference between the top and bottom of the layer >2 K. If a layer meets this criterion, the Heffter method places the PBLH at the top of this layer. Otherwise, the PBLH is set to the altitude of the maximum potential temperature lapse rate below 4 km. If there are no lapse rate values $>5 \frac{K}{km}$, the PBLH is indeterminate.

The Heffter method and other automated PBLH retrieval methods using radiosondes fail in certain conditions. Frequently, potential temperature inversion layers at the PBLH do not meet the criteria for the Heffter method, and the automated retrieval method sets the PBLH to the top of an RL. Thus, the PBLH is routinely estimated by inspection of radiosonde potential temperature profiles,[30] and the radiosonde PBLH is adjusted to these lower inversion layers in these cases.

4 Results

Two cases with different boundary layer conditions are presented to demonstrate the effectiveness of the HWT technique using MPD data. On each day, radiosondes were launched for comparison. The first day presented, March 13, 2021, demonstrates a well-behaved boundary layer with one significant aerosol gradient. The second day, June 2, 2021, demonstrates a more complicated boundary layer regime with a strong morning CI and a turbulent evening transition.

4.1 Case Study 1: March 13, 2021

Figure 4 shows the boundary layer regimes in terms of the aerosol backscatter coefficient, β_{aer}, on a logarithmic scale for data collected on March 13, 2021. Sunrise is at 6:39 MST, and sunset is at 18:27 MST. In the first few hours of the morning, the PBLH is below the minimum range of the lidar. An RL is present in the morning, but the top limiter prevents the algorithm from selecting the CI. At 9:30 MST, the PBLH rises above the minimum range of the lidar, reaching a maximum height of 880 m at 12:30 MST. The PBLH is relatively constant until the last hour
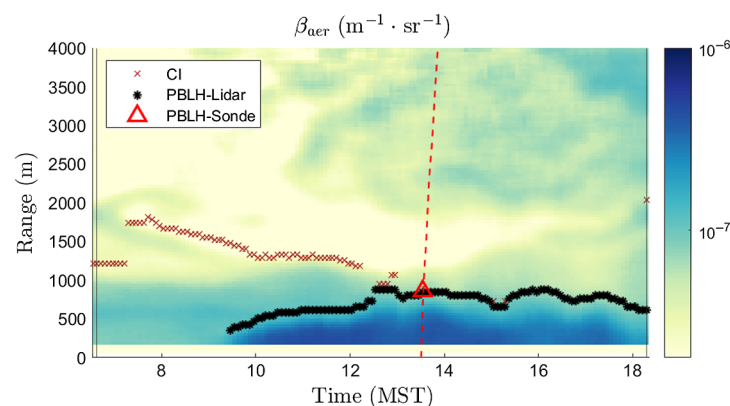

Fig. 4 The aerosol backscatter coefficient taken on March 13, 2021, from sunrise to sunset with the PBLH and the CI. The red-dashed line represents a radiosonde launch.
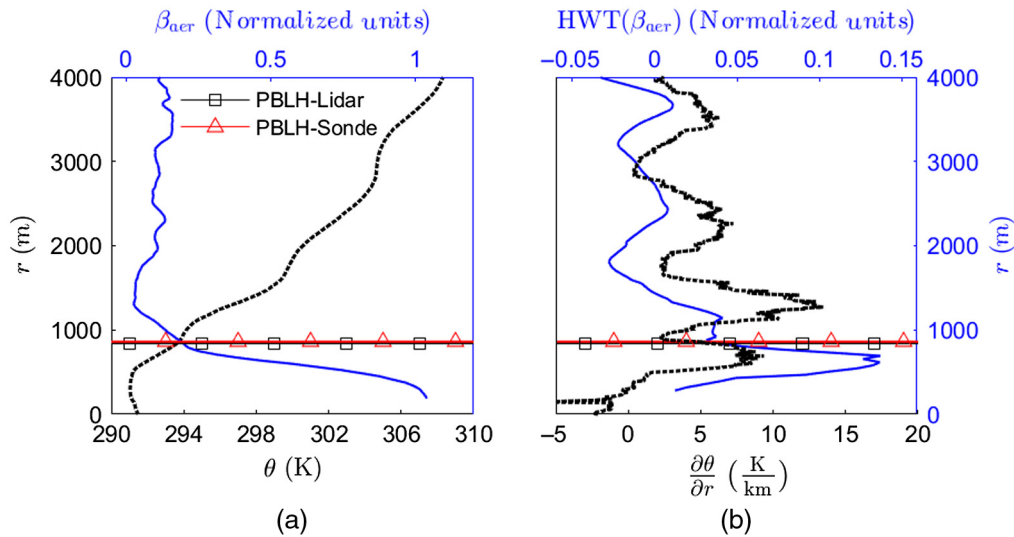
Fig. 5 A radiosonde launch with PBLH values found by lidar and radiosonde methods taken on March 13, 2021, 13:30 MST. (a) The aerosol backscatter coefficient (potential temperature) as the blue solid (black dotted) line. (b) The HWT (potential temperature lapse rate) as the blue solid (black dotted) line.

before sunset when it begins to descend. A weak RL is present in the afternoon. However, this layer had few aerosols, and the HWT value at the top of this layer did not meet the 0.05 threshold of the CI, and the retrieval algorithm placed the CI at the PBLH.

A radiosonde was launched at 13:30 MST and is indicated in Fig. 4 as the red-dashed line. The radiosonde potential temperature, θ, and aerosol backscatter coefficient, β_{aer}, profiles, are shown in Fig. 5(a). The potential temperature lapse rate, $\frac{\partial \theta}{\partial r}$, and the HWT of the aerosol back-scatter coefficient are shown in Fig. 5(b). The HWT shows a single transition layer, and the PBLH from the HWT method is 843 m. In the potential temperature profile, there are several inversion layers. The lowest inversion layer is located at the same altitude as the aerosol transition layer. The PBLH determined by the radiosonde profile is 861 m, closely matching the PBLH determined by the HWT method.

4.2 Case Study 2: June 2, 2021

Figure 6 shows the boundary layer regimes in terms of the aerosol backscatter coefficient on a logarithmic scale for data collected on June 2, 2021. Sunrise is at 5:37 MDT, and sunset is at
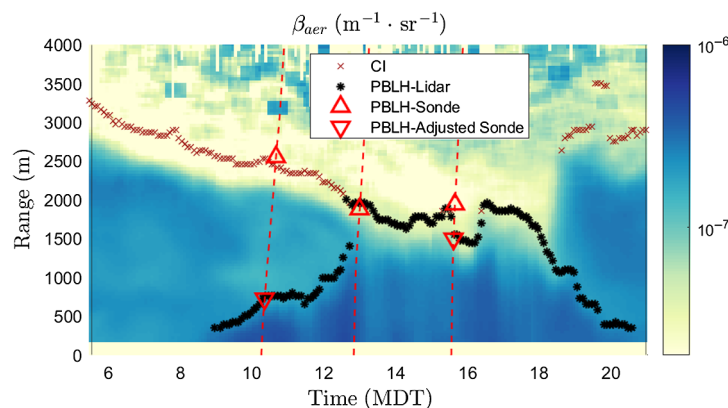

Fig. 6 The aerosol backscatter coefficient taken on June 2, 2021, with the PBLH and CI. The red-dashed lines represent radiosonde launches.

21:07 MDT. Three radiosondes were launched and are shown as red-dashed lines. There is a strong RL in the first few hours of the morning, but the top limiter prevents the algorithm from selecting the CI. At about 8:30 MDT, the PBLH rises above the minimum range of the lidar and reaches a maximum height of 2004 m at 12:38 MDT. The PBLH remains relatively constant until ~17:15 MDT when it begins to descend. Turbulence in the evening transition period creates an RL, but the top limiter prevents the HWT from choosing this layer. The PBLH descends until sunset. It is last detected at 356 m at 20:33 MDT.

For the radiosonde launched at 10:15 MDT, the potential temperature and the aerosol backscatter coefficient profiles are shown in Fig. 7(a), while the potential temperature lapse rate and the HWT are shown in Fig. 7(b). The HWT shows two clear aerosol transition layers. The first is associated with the PBLH and the second is the top of an RL. The top limiter is below this RL, so the HWT method places the PBLH at 768 m. The potential temperature profile shows two clear inversions at the same altitudes as the aerosol transition layers. However, the lowest inversion does not have a potential temperature difference of 2 K between the top and the bottom of the layer, so the Heffter method selects the second one as the PBLH. The Heffter method PBLH is 2552 m. This altitude is the top of an RL, so the PBLH from the potential temperature profile is adjusted to the top of the lower inversion layer at 727 m. The adjusted PBLH from the potential temperature profile closely matches the PBLH as derived by the HWT method.

For the radiosonde launched at 12:49 MDT, the potential temperature and the aerosol backscatter coefficient profiles are shown in Fig. 7(c), while the potential temperature lapse rate and the HWT of the aerosol backscatter profiles are shown in Fig. 7(d). The HWT shows a single aerosol transition layer. The HWT method locates the PBLH to be 1967 m. The potential temperature profile from the radiosonde shows the lowest significant potential temperature inversion to be located at the same altitude as the aerosol transition layer. The PBLH determined by the potential temperature profile is 1879 m, which closely matches the PBLH as determined by the HWT method.

For the radiosonde launched at 15:32 MDT, the potential temperature and the aerosol backscatter coefficient profiles are shown in Fig. 7(e), while the potential temperature lapse rate and the HWT are shown in Fig. 7(f). The HWT shows a single significant aerosol transition layer. The PBLH as determined by the HWT method is 1555 m. The potential temperature profile shows several significant inversion layers. The lowest potential temperature inversion layer is located at approximately the same altitude as the aerosol transition layer. None of the inversion layers met the criterion that the difference in potential temperature between the top and the bottom of the inversion layer be >2 K, so the Heffter method places the PBLH at the point where the potential temperature lapse rate reaches a maximum. The Heffter method places the PBLH at 1943 m. However, because there is an obvious potential temperature inversion layer below this, this inversion layer is not the PBLH. The PBLH, as determined by radiosonde, is adjusted to the top of the lower layer, with an altitude of 1499 m. This adjusted radiosonde PBLH matches the HWT method closely. This radiosonde was launched at almost the exact time that the HWT method jumped between aerosol transition layers. This jump can be seen in Fig. 6, where the PBLH, as determined by the HWT method, followed the second inversion layer until the sonde was launched, then switched to the first layer as the aerosol transition layer shifted lower in altitude. This radiosonde highlights how the choice of thresholds affects the PBLH retrieval in both the lidar and radiosonde methods.

4.3 Radiosonde Comparisons

Radiosondes were used to compare the HWT method to a potential temperature method. About 32 radiosondes were launched between March and September 2021. Initially, the Heffter method was used for comparison. However, many potential temperature inversion layers near the PBLH found by the HWT method were too weak to be located by the Heffter method. The Heffter criteria are often too strict, and the Heffter method frequently misses the potential temperature inversion layer at the PBLH. Additionally, the Heffter method has no top limiter other than 4 km, so the Heffter method frequently places the PBLH at the top of an RL.

The PBLH values found using the Heffter method compared with the HWT method is shown in Fig. 8(a). Out of the 32 radiosondes launched, no potential temperature inversion layer met the
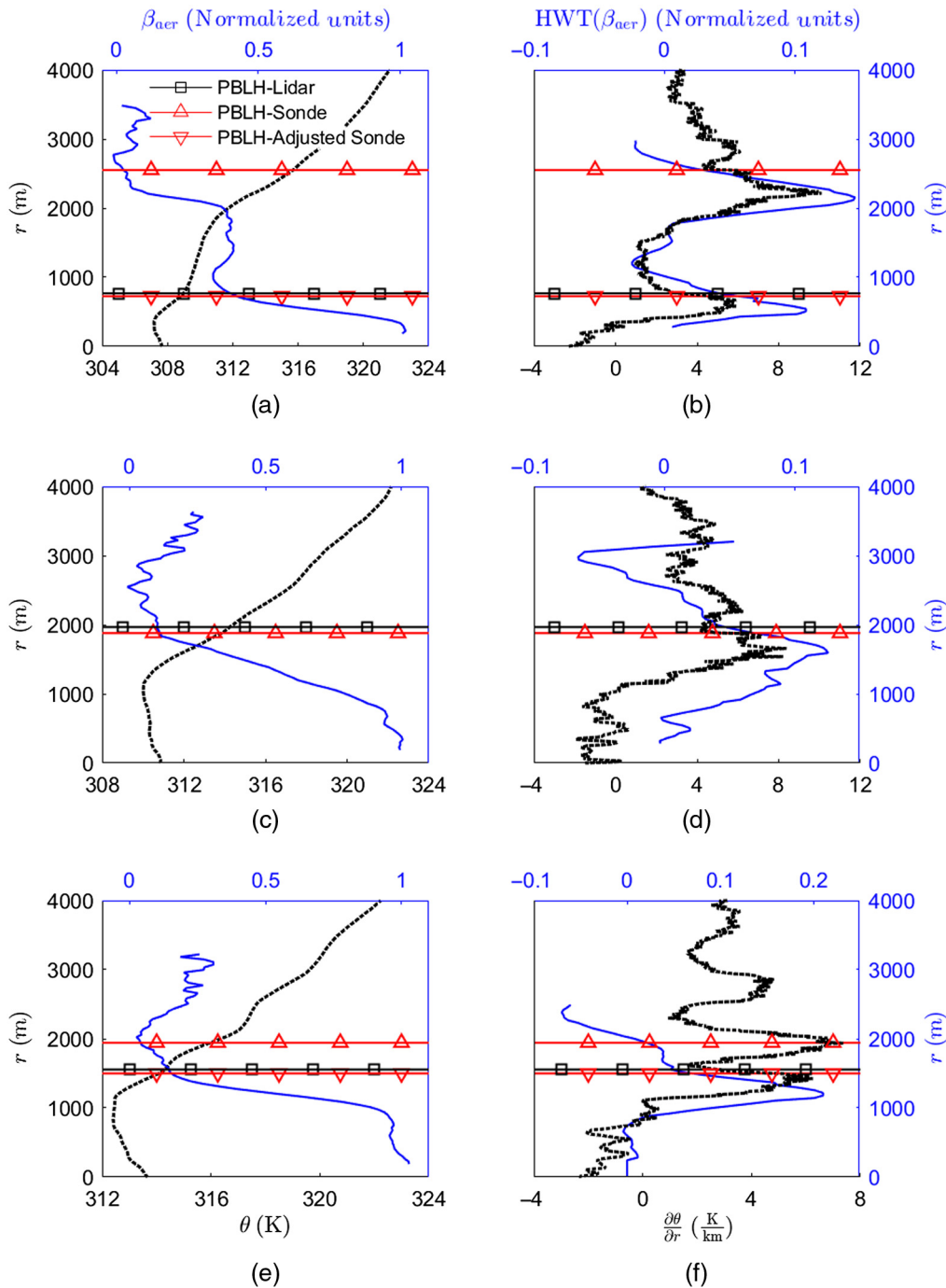
Fig. 7 Radiosonde launches with PBLH values found by lidar and radiosonde methods on June 2, 2021. (a) The aerosol backscatter coefficient (potential temperature) as the blue solid (black dotted) line for the sonde launched at 10:15 MDT. (b) The HWT (potential temperature lapse rate) as the blue solid (black dotted) line for the sonde launched at 10:15 MDT. (c) The same as (a) for the sonde launched at 12:49 MDT. (d) The same as (b) for the sonde launched at 12:49 MDT. (e) The same as (a) for the sonde launched at 15:32 MDT. (f) The same as (b) for the sonde launched at 15:32 MDT.

Heffter method criteria in eight radiosonde profiles. Of the remaining 24 profiles, the Heffter method and the HWT method located the same inversion layer nine times and located different inversion layers 15 times. The nine cases where the two methods agree on which inversion layer is the PBLH closely agree. The PBLH, as found by the HWT method, is, on average, 105 m below the PBLH as found by the Heffter method when the methods agree. The linear model for
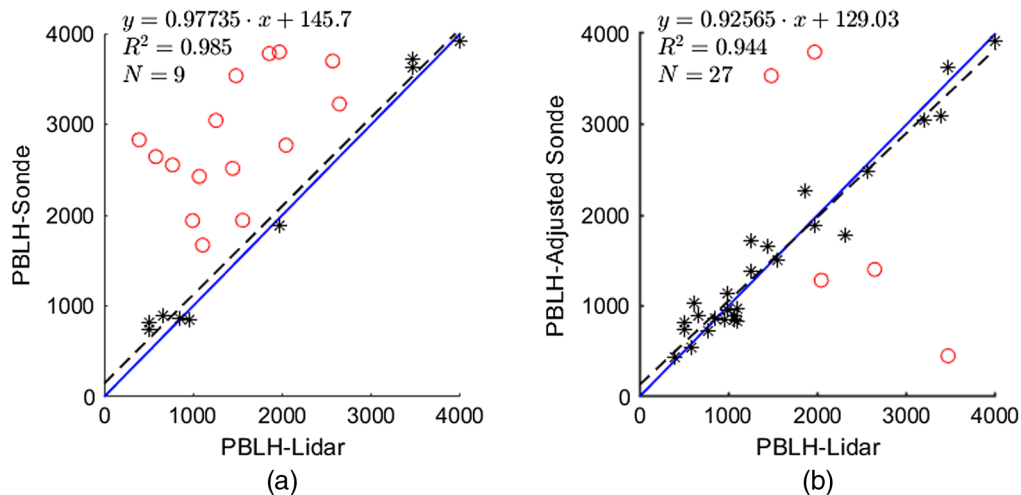
Fig. 8 Comparison between the lidar and radiosonde PBLH values. (a) A comparison between the HWT and Heffter PBLH values. The black asterisks represent sonde launches where the methods chose the same inversion layers as the PBLH, and the red circles represent sonde launches where the two methods chose different inversion layers as the PBLH. The black dotted line is a linear fit for the black asterisks, and the blue solid line is a 1 to 1 line for comparison. (b) The same as (a), except the lidar and adjusted radiosonde PBLH values are compared.

sonde launches where the methods agreed has an offset of 146 m, a slope of 0.977, and a coefficient of determination of $R^2 = 0.985$.

The PBLH was adjusted to the height of the lowest potential temperature inversion layer for the radiosonde profiles in cases when the Heffter method missed low-altitude inversion layers. The adjusted PBLH values found by radiosonde and the PBLH values found by the HWT method are shown in Fig. 8(b). Of the 32 radiosonde launches, the PBLH was visible in every launch. The PBLH, as determined by the HWT method and the adjusted radiosonde PBLH, were located at the same inversion layer in 27 launches. The other five launches included two where the HWT method located a spurious layer underneath the PBLH with an extended transition zone, two where the HWT method located the top of an RL, and one where the PBLH below a cloud layer was not detected. There were slightly elevated potential temperature lapse rates near the spurious aerosol layers, but they were too weak to be the correct PBLH. For the 27 radiosondes where the two methods chose the same layer, the PBLH, as found by the HWT method, was on average 18 m lower than the PBLH determined from the potential temperature profile. The linear model for these radiosonde launches has an offset of 129 m, a slope of 0.926, and a coefficient of determination of $R^2 = 0.944$.

5 Discussion

An automated algorithm for determining the PBLH from MPD data has been developed and demonstrated and has the potential to add a valuable data product to the MPD network currently in development. Using the HWT method with a top limiter and special conditions for clouds, the automated retrieval algorithm finds the PBLH using MPD data for most conditions. The thresholds and the range-dependent dilation equation used in this paper were only tested for Bozeman, Montana, and will not necessarily work well for other locations and thus requires further field validation experiments. The most common error results when the HWT method locates a spurious aerosol layer in the case of an extended PBLH and underestimates the PBLH. Another frequent error occurs when the HWT fails to locate an RL and errantly sets the PBLH to the top of an RL. These issues are not unique to lidar retrieval algorithms; the Heffter method, which uses the potential temperature profile from radiosonde launches, frequently mistakes the top of an RL for the PBLH.

The MPD contains a water vapor differential absorption lidar for profiling atmospheric water vapor concentrations in addition to the HSRL and the oxygen differential absorption lidar for temperature profiling. The retrieval algorithm in this paper only uses data from the HSRL, but future work will explore using the water vapor and temperature profiling capabilities of the MPD for improving the PBLH retrieval algorithms.

6 Conclusion

The MPD is valuable for continuous monitoring of the thermodynamics of the lower troposphere. This paper demonstrated using an HSRL built with the MPD architecture to monitor the daytime PBLH with an automatic retrieval algorithm. The PBLH is a data product that improves the utility of the MPD network and could be used for weather forecasting or forecasting pollution events. The retrieval algorithm used the HWT of the normalized aerosol backscatter coefficient, a range-dependent dilation, and a top limiting algorithm. The PBLH, as found by the HWT method, closely matched the PBLH determined from the potential temperature profiles from radiosonde launches. For 27 of the 32 radiosonde launches, the two methods selected the same inversion layer as the PBLH. For these launches, the PBLH as determined by the HWT method was on average 18 m below the PBLH as determined by radiosonde. The linear fit has a coefficient of determination of $R^2 = 0.944$. Additionally, the HWT method using MPD data was more effective than the Heffter method at tracking the lowest aerosol layer associated with the PBLH.

Acknowledgments

References

1. R. B. Stull, *An Introduction to Boundary Layer Meteorology*, Kluwer Academic, Dordrecht, Netherlands (1988).
2. M. Lothon et al., "The BLLAST field experiment: boundary-layer late afternoon and sunset turbulence," *Atmos. Chem. Phys.* **14**(20), 10931–10960 (2014).
3. K. Browning et al., "The convective storm initiation project," *Bull. Am. Meteorol. Soc.* **88**, 1939–1956 (2007).
4. C. Draxl et al., "Evaluating winds and vertical wind shear from weather research and forecasting model forecasts using seven planetary boundary layer schemes," *Wind Energy* **17**(1), 39–55 (2014).
5. O. Krogsæter and J. Reuder, "Validation of boundary layer parameterization schemes in the weather research and forecasting model under the aspect of offshore wind energy applications, part I: average wind speed and wind shear," *Wind Energy* **18**(5), 769–782 (2015).
6. J. C. Lin et al., "A near-field tool for simulating the upstream influence of atmospheric observations: the stochastic time-inverted Lagrangian transport (STILT) model," *J. Geophys. Res. Atmos.* **108**(D16), ACH-1–ACH-17 (2003).
7. X.-M. Hu, J. W. Nielsen-Gammon, and F. Zhang, "Evaluation of three planetary boundary layer schemes in the WRF model," *J. Appl. Meteorol. Climatol.* **49**(9), 1831–1844 (2010).
8. X. Huang et al., "Chemical boundary layer and its impact on air pollution in northern China," *Environ. Sci. Technol. Lett.* **7**(11), 826–832 (2020).
9. T. M. Bell et al., "Confronting the boundary layer data gap: evaluating new and existing methodologies of probing the lower atmosphere," *Atmos. Meas. Tech.* **13**(7), 3855–3872 (2020).
10. H. Baars et al., "Continuous monitoring of the boundary-layer top with lidar," *Atmos. Chem. Phys.* **8**(23), 7281–7296 (2008).

11. J. D. Hegarty et al., "Analysis of the planetary boundary layer height during discover-AQ Baltimore-Washington, D.C., with lidar and high-resolution wrf modeling," *J. Appl. Meteorol. Climatol.* **57**(11), 2679–2696 (2018).

12. R. Dang et al., "Atmosphere boundary layer height (ABLH) determination under multiple-layer conditions using micro-pulse lidar," *Remote Sens.* **11**(3), 263 (2019).

13. L. Menut et al., "Urban boundary-layer height determination from lidar measurements over the Paris area," *Appl. Opt.* **38**, 945–954 (1999).

14. K. Hayden et al., "The vertical chemical and meteorological structure of the boundary layer in the lower Fraser valley during pacific '93," *Atmos. Environ.* **31**(14), 2089–2105 (1997).

15. I. M. Brooks, "Finding boundary layer top: application of a wavelet covariance transform to lidar backscatter profiles," *J. Atmos. Ocean. Technol.* **20**(8), 1092–1105 (2003).

16. S. A. Cohn and W. M. Angevine, "Boundary layer height and entrainment zone thickness measured by lidars and wind-profiling radars," *J. Appl. Meteorol.* **39**(8), 1233–1247 (2000).

17. D. G. Steyn, M. Baldi, and R. M. Hoff, "The detection of mixed layer depth and entrainment zone thickness from lidar backscatter profiles," *J. Atmos. Ocean. Technol.* **16**(7), 953–959 (1999).

18. C. Münkel et al., "Retrieval of mixing height and dust concentration with lidar ceilometer," *Bound.-Layer Meteorol.* **124**, 117–128 (2007).

19. A. K. Piironen and E. W. Eloranta, "Convective boundary layer mean depths and cloud geometrical properties obtained from volume imaging lidar data," *J. Geophys. Res. Atmos.* **100**(D12), 25569–25576 (1995).

20. A. Lammert and J. Bösenberg, "Determination of the convective boundary-layer height with laser remote sensing," *Bound.-Layer Meteorol.* **119**, 159–170 (2006).

21. L. Colberg et al., "Planetary boundary layer height measurements using diode-laser-based high spectral resolution lidar," in *102nd Am. Meteorol. Soci. Annu. Meeting*, AMS (2022).

22. O. Cruikshank et al., "Micropulse differential absorption lidar for temperature retrieval in the lower troposphere," in *102nd Am. Meteorol. Soci. Annu. Meeting*, AMS (2022).

23. R. A. Stillwell et al., "A field-deployable diode-laser-based micropulse lidar system to measure atmospheric thermodynamic variables: field testing," in *102nd Am. Meteorol. Soci. Annu. Meeting*, AMS (2022).

24. S. M. Spuler et al., "Micropulse dial (MPD)—a diode-laser-based lidar architecture for quantitative atmospheric profiling," *Atmos. Meas. Tech.* **14**(6), 4593–4616 (2021).

25. R. A. Stillwell et al., "Demonstration of a combined differential absorption and high spectral resolution lidar for profiling atmospheric temperature," *Opt. Express* **28**, 71–93 (2020).

26. M. Hayman and S. Spuler, "Demonstration of a diode-laser-based high spectral resolution lidar (HSRL) for quantitative profiling of clouds and aerosols," *Opt. Express* **25**, A1096–A1110 (2017).

27. I. Binietoglou et al., "A methodology for cloud masking uncalibrated lidar signals," *EPJ Web Conf.* **176**, 05048 (2018).

28. D. Toledo et al., "Estimation of the atmospheric boundary layer height during different atmospheric conditions: a comparison on reliability of several methods applied to lidar measurements," *Int. J. Remote Sens.* **38**, 3203–3218 (2017).

29. C. Sivaraman et al., "*Planetary boundary layer (PBL) height value added product (VAP): radiosonde retrievals*," Tech. Rep. 1, Office of Science, U.S. Department of Energy (2013).

30. P. Seibert et al., "Review and intercomparison of operational methods for the determination of the mixing height," *Atmos. Environ.* **34**(7), 1001–1027 (2000).

Luke Colberg is a graduate student in the Electrical and Computer Engineering Department at Montana State University currently pursuing a PhD in electrical engineering. He received his BS degree in mechanical engineering and his MS degree in optics and photonics from Montana State University in 2019 and 2021. His research area is optical remote sensing.

Owen Cruikshank is a graduate student in the Electrical and Computer Engineering Department at Montana State University pursuing a PhD in electrical engineering. He received his BS degree in physics from Michigan Technological University in 2018 and his MS degree in

optics and photonics from Montana State University in 2021. His research area is optical remote sensing.

Kevin S. Repasky received his BSEng degree in mechanical engineering from Youngstown State University in 1988 and his MS and PhD degrees in physics from Montana State University in 1992 and 1996, respectively. Currently, he is a professor in the Electrical and Computer Engineering Department at Montana State University. His research interests include laser design and development, nonlinear optics, optical remote sensing, and optical communications.